J Solid State Electrochem (2012) 16:1279–1290
DOI 10.1007/s10008-011-1520-7

ORIGINAL PAPER

Electrochemical characterization of polypyrrole–$LiNi_{1/3}Mn_{1/3}Co_{1/3}O_2$ composite cathode material for aqueous rechargeable lithium batteries

R. B. Shivashankaraiah · H. Manjunatha · K. C. Mahesh · G. S. Suresh · T. V. Venkatesha

Received: 9 May 2011 / Revised: 5 July 2011 / Accepted: 1 August 2011 / Published online: 17 August 2011

Abstract A series of polypyrrole (PPy)–$LiNi_{1/3}Mn_{1/3}Co_{1/3}O_2$ composite electrodes are formed by physical mixing of polypyrrole with $LiNi_{1/3}Mn_{1/3}Co_{1/3}O_2$ cathode material. $LiNi_{1/3}Mn_{1/3}Co_{1/3}O_2$ is synthesized by reaction under autogenic pressure at elevated temperature method. Highly resolved splitting of 006/102 and 108/110 peaks in the XRD pattern provide an evidence to well-ordered layered structure of the compound. The ratios of the intensities of 003 and 104 peaks are found to be >1, which indicate no pronounced mixing of the cation. Cyclic voltammetry and AC impedance studies revealed that the addition of polypyrrole significantly decreases the charge-transfer resistance of $LiNi_{1/3}Mn_{1/3}Co_{1/3}O_2$ electrodes. The electrochemical reactivity of PPy–$LiNi_{1/3}Mn_{1/3}Co_{1/3}O_2$ composite electrode is examined during lithium ion insertion and de-insertion by galvanostatic charge–discharge testing; 10 wt.% PPy–$LiNi_{1/3}Mn_{1/3}Co_{1/3}O_2$ composite electrode exhibits better electrochemical performance by increasing the reaction reversibility and capacity compared to that of the pristine $LiNi_{1/3}Mn_{1/3}Co_{1/3}O_2$ electrode. The cell with 10 wt.% PPy added cathode shows significant improvement in the electrochemical performance compared with that having pristine cathode. The capacity remains about 70% of the initial value after 50 cycles while for cell with pristine cathode only about 28% of initial capacity remains after 40 cycles.

Keywords Polypyrrole · Cathode material · Aqueous lithium-ion batteries · AC impedance spectroscopy

R. B. Shivashankaraiah · H. Manjunatha · K. C. Mahesh · G. S. Suresh (✉)
Chemistry Research Centre, S. S. M. R. V. Degree College, Jayanagar,
Bangalore 560041, India
e-mail: sureshssmrv@yahoo.co.in

T. V. Venkatesha
Department of Chemistry, Kuvempu University, Jnanasahyadri, Shankaraghatta,
577451, Shimoga, India

Introduction

Aqueous rechargeable lithium batteries proposed by Dahn and coworkers [1] are found to have some advantages over non-aqueous systems. Compared with non-aqueous lithium ion battery, in aqueous lithium ion batteries, the safety issue is essentially settled, severe manufacturing conditions are ignored, and the conductivity of aqueous solutions is two orders of magnitude higher than that of organic electrolytes. Although the energy density of these batteries is lower than that of non-aqueous lithium ion batteries, it can be compared with that of Pb-acid and Ni–Cd batteries [2]. Poor cycle performance of this battery system is the major concern preventing its wide investigation and application. The reason for the capacity loss is not clear, though many researchers have devoted their work towards studying different electrode materials and their fundamental performances in aqueous cells [3–6].

In order to replace traditional cathode materials, many new material systems have been developed in non-aqueous lithium ion batteries [7]. Among such systems, $LiNi_{1/3}Mn_{1/3}Co_{1/3}O_2$ is the most unique one because it contains equal molarities of Ni, Co, and Mn. In this solid solution, the valence states of Ni, Mn, and Co are 2+, 4+, and 3+, respectively. Layered $LiNi_{1/3}Mn_{1/3}Co_{1/3}O_2$ is a solid solution of $LiCoO_2$, and $LiNi_{0.5}Mn_{0.5}O_2$ has been paid much attention as a cathode material for lithium ion batteries due to its higher reversible

capacity, lower cost, and less toxicity than commercially used $LiCoO_2$. During charge–discharge process, only divalent Ni and trivalent Co can take part in redox process and tetravalent Mn ion is inactive, which is believed to support the host structure during redox process [8].

Since Ohzuku et.al synthesized $LiNi_{1/3}Mn_{1/3}Co_{1/3}O_2$ by solid-state reaction method [9], many attempts have been made to prepare and explore the possibilities of using this layered compound as a cathode material in rechargeable lithium ion batteries [10–13]. This material has been demonstrated to possess high discharge capacity, good thermal stability, and excellent cycling stability [14–17]. Many research groups have adopted the solid-state method to prepare $LiNi_{1/3}Mn_{1/3}Co_{1/3}O_2$ powders [18]. However, $LiNi_{1/3}Mn_{1/3}Co_{1/3}O_2$ derived from the solid-state method faces problems of irreversible charge–discharge behavior. The irreversible capacity problem may be conquered in two ways: one is to alter the starting materials or heating conditions and the other is to employ other synthesis methods [19]. Therefore, in this study, a simple heating method called reaction under autogenic pressure at elevated temperature (RAPET) method employing the use of a stainless steel cell was adapted to synthesize $LiNi_{1/3}Mn_{1/3}Co_{1/3}O_2$ powders. This method has the advantages in controlling particle size, morphology, and lowering reaction temperature for the prepared powders.

The investigation on improvement of cycle life of aqueous lithium batteries is found to be more interesting. Electronically conducting polymers such as polypyrrole, polyaniline, and polythiophene have been used to form composite cathode materials such as $LiMn_2O_4$–PPy [20] and V_2O_5–PAni [21] to improve the conductivity, coulombic efficiency, rate capability, and stabilize the cycle capacity of the electrode material. In case of $LiMn_2O_4$–PPy composite, the addition of polypyrrole increases the capacity of the pure $LiMn_2O_4$ from 110 to 125 mAh g^{-1}. The conducting polymer coating on transition metal oxides stabilize the cycling capacity of the electrode, thus enhancing the cycle life of the aqueous lithium ion cell. Polypyrrole is known as an inherent electrically conducting polymer due to the conjugation of the single and double bonds alternating within the macromolecular architecture. The extra electrons of the double bond in a conjugated system are free to move through the polymer chain inducing electrical conductivity. It also acts as a binder and is known to stabilize the cycling capacity of electrodes. With such an idea, we prepared $LiNi_{1/3}Mn_{1/3}Co_{1/3}O_2$–PPy composite electrode using physical admixing method, and it was used as a cathode material for an aqueous rechargeable lithium battery. LiV_3O_8 and 5 M $LiNO_3$ aqueous solution were used as anode and electrolyte, respectively. Here, we report the electrochemical synthesis of polypyrrole and its effect as an additive on the performance of $LiNi_{1/3}Mn_{1/3}Co_{1/3}O_2$ cathode material. Cyclic voltammetry (CV), galvanostatic charge–discharge, and electrochemical impedance spectroscopy techniques were used to investigate the effect of polypyrrole addition to $LiNi_{1/3}Mn_{1/3}Co_{1/3}O_2$. We also evaluate the kinetic parameters of lithium ion at bare $LiNi_{1/3}Mn_{1/3}Co_{1/3}O_2$ and at PPy–$LiNi_{1/3}Mn_{1/3}Co_{1/3}O_2$ composite electrodes.

Experimental

Synthesis of electrode materials

$LiNi_{1/3}Mn_{1/3}Co_{1/3}O_2$ cathode material was synthesized by RAPET method. In a typical procedure, stoichiometric amounts of LiOH, MnO_2, $NiCO_3$, and $Co(OH)_2$ (all from Sigma–Aldrich) are mixed, ground well, and pressed into pellets. The resulting powder is introduced into a 5-ml swagelok cell. The Swagelok parts consist of a small threaded tube closed by two caps from both sides. The filled Swagelok is closed tightly in oxygen environment and placed inside an alumina pipe in the middle of the furnace. The temperature is raised at a rate of 10 °C/min to 600 °C and held at this temperature for 10 h. The chemical dissociation and transformation reaction takes place under the autogenic pressure of the precursors at the fixed temperature. The Swagelok cell is allowed to cool gradually to room temperature, opened and the obtained products are used after grinding. LiV_3O_8 anode material was synthesized by a conventional solid-state reaction by heating a stoichiometric mixture of LiOH and V_2O_5 to a temperature of 680 °C. The resulting melt was quenched to room temperature leading to a brown solid consisting of crystalline LiV_3O_8 particles.

Powder X-ray diffraction (XRD) patterns of the synthesized electrode materials were recorded using a Philips X'pert Pro diffractometer with CuKα (λ=1.5418 Å) as the source. Scanning electron microscopy (Zeisf Model Supra, Germany) was used to observe surface morphology of $LiNi_{1/3}Mn_{1/3}Co_{1/3}O_2$.

Electrochemical synthesis of polypyrrole

Polypyrrole was electrochemically synthesized on platinum substrate by multiple potential cycling (20 cycles) between −1.0 and 1.1 V vs saturated calomel electrode at a sweep rate of 50 mV s^{-1} in 0.1 M pyrrole monomer aqueous solution containing 0.1 M KCl as supporting electrolyte. When the electro polymerization was accomplished, the PPy–coated electrode was removed from the monomer solution and washed thoroughly with water for several times, dried and the PPy obtained was used as an additive for $LiNi_{1/3}Mn_{1/3}Co_{1/3}O_2$ material.

Electrochemical measurements

The cathode and anode electrode preparation was conducted in the same way as follows. Stainless steel mesh was used as current collector. The mesh was cut into circular shape of about 1 cm^2 area and welded with stainless steel wire for electrical contact. The mesh was sandblasted to remove the oxide layer, washed with water, rinsed with acetone, dried, and weighed. Powder mixture of the sample, carbon black, and polytetafluoroethylene in the weight ratio 80:10:10 were ground in a mortar; a few drops of NMP were added to get slurry. The slurry was coated onto the pretreated mesh and dried in a vacuum oven at 110 °C overnight. The loading of the electrode material was around 10 mg cm^{-2}.

A three-electrode electrochemical cell was employed for CV study in aqueous 5 M $LiNO_3$ solution. A saturated calomel electrode (SCE) and Pt foil were used as reference and counter electrodes, respectively. Electrochemical impedance measurements were carried out potentiometrically using a three-electrode system with an AC excitation signal of 10 mV over the frequency range from 100 kHz to 5 mHz. Galvanostatic charge–discharge experiments were carried out using $LiNi_{1/3}Mn_{1/3}Co_{1/3}O_2$ and $LiNi_{1/3}Mn_{1/3}Co_{1/3}O_2$–PPy as cathodes and LiV_3O_8 as anode. All the electrochemical measurements were carried out using the Biologic potentiostat–galvanostat instrument.

Results and discussion

Characterization of cathode, anode, and polypyrrole materials by XRD FT–IR and cyclic voltammetry techniques

Figure 1a shows the scanning electron microscope image of $LiNi_{1/3}Mn_{1/3}Co_{1/3}O_2$ obtained by RAPET method. The well-dispersed crystalline particles are observed and the reaction takes place at autogenic pressure at elevated temperature that reduces the synthesis time and shortens the particle size. Most of the particles have non-spherical shape and sizes less than 200 nm. Figure 1b shows the XRD patterns of synthesized $LiNi_{1/3}Mn_{1/3}Co_{1/3}O_2$ and LiV_3O_8 electrode materials. $LiNi_{1/3}Mn_{1/3}Co_{1/3}O_2$ has a rhombohedral structure belonging to the *R3m* space group of hexagonal-$NaFeO_2$ structure. The low values of *R* factor, $R = (I_{102} + I_{101})/I_{101}$ relating to the integrated intensities of the corresponding well-resolved peaks of the material also confirm their hexagonal ordering. Highly resolved splitting of 006/102 and 108/110 peaks provide an evidence of a characteristic well-ordered layered structure of the compound. The ratios of the intensities of 003 and 104 peaks in the XRD pattern were found to be >1. This may

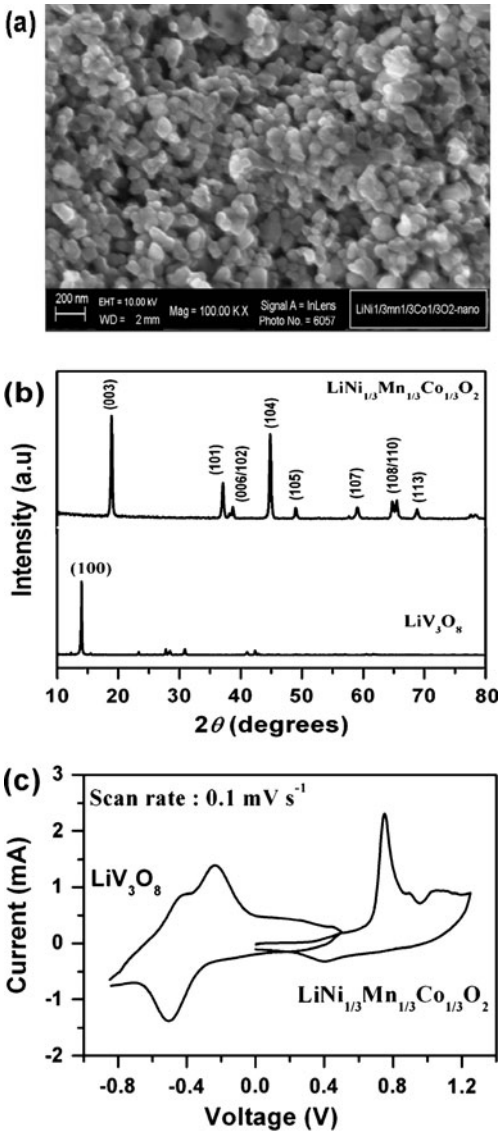

Fig. 1 **a** Scanning electron micrograph of $LiNi_{1/3}Mn_{1/3}Co_{1/3}O_2$ particles, **b** X-ray diffraction pattern of synthesized $LiNi_{1/3}Mn_{1/3}Co_{1/3}O_2$ and LiV_3O_8, **c** CV profiles of $LiNi_{1/3}Mn_{1/3}Co_{1/3}O_2$ and LiV_3O_8 in 5 M $LiNO_3$ solution with a scan rate of 0.1 mV s^{-1} vs SCE

indicate no pronounced cation mixing. We conclude from this XRD results that there are no remarkable impurities in the materials obtained. The γ-phase of LiV_3O_8 is generally described as non-stoichiometric $Li_{1+x}V_3O_8$ or LiV_3O_{8-y} (with x, $y<1$) containing a slight amount of V (IV) [22, 23]. The $Li_{1+x}V_3O_8$ is referred to as LiV_3O_8 here for simplification due to the neglecting influence of the existing V^{4+} cations on the reported properties of the compound. Crystalline γ-LiV_3O_8 can be obtained by cooling a melt of a stoichiometric mixture of lithium and vanadium salts. From Fig. 1b, it is clear that the obtained LiV_3O_8 already exhibits a high degree of crystallinity. The largest peak at about $2\theta=13°$ is assigned to the diffraction at the (100) plane indicating the layered structure of LiV_3O_8. These

layers consist of VO_6 octahedral and VO_5 trigonal bipyramidal which are corner sharing with the octahedral. The Li^+ cations are assumed to be intercalated between such layers [23]. In the X-ray diffraction pattern, only reflexes of LiV_3O_8 (or $Li_{1+x}V_3O_8$ with $x \ll 1$) can be detected. Therefore, the synthesis method used is appropriate to produce crystalline LiV_3O_8 as a main product.

The cyclic voltammogram of $LiNi_{1/3}Mn_{1/3}Co_{1/3}O_2$ prepared by RAPET method and LiV_3O_8 synthesized by solid-state method in 5 M $LiNO_3$ aqueous solution are as shown in Fig. 1c. $LiNi_{1/3}Mn_{1/3}Co_{1/3}O_2$ exhibits a sharp intense anodic peak centered at 0.75 V corresponding to the de-intercalation of lithium ions and a cathodic peak at 0.40 V corresponding to the lithium ion intercalation reaction. During this process, no oxygen evolution peak can be observed which is obviously due to the over potential of the electrode. The average redox potential is 0.57 V. The oxygen evolution takes place above 1.25 V. This shows that it is possible to remove lithium ions from the material before the evolution of oxygen. Thus, it is possible to use the prepared $LiNi_{1/3}Mn_{1/3}Co_{1/3}O_2$ as cathode material in the aqueous solution without much oxygen evolution. For LiV_3O_8, lithium ion intercalation peak can be observed at

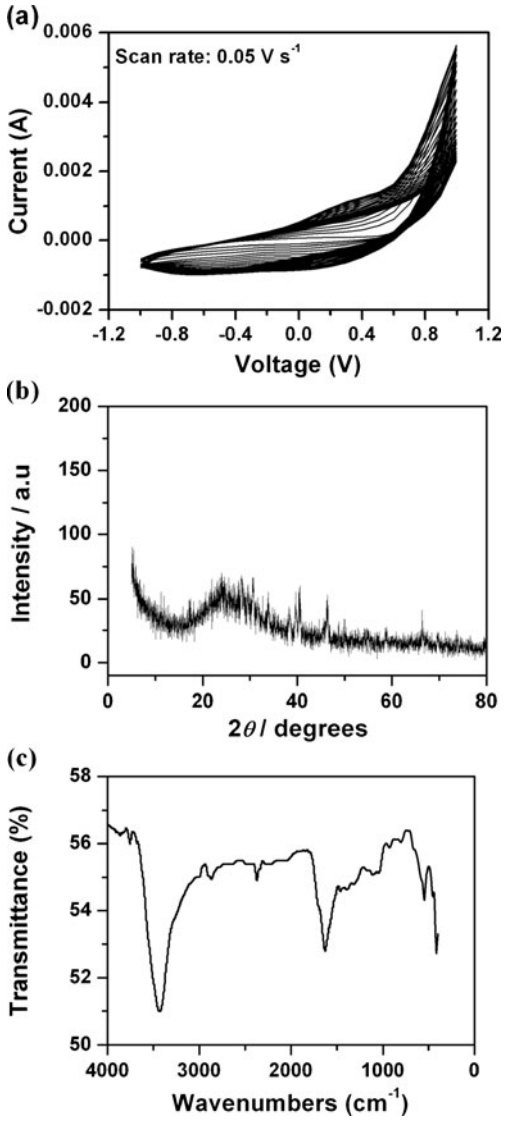

Fig. 2 **a** Cyclic voltammogram for the formation of polypyrrole (PPy) in 0.1 M pyrrole monomer containing 0.1 M KCl aqueous solution on Pt substrate. **b** XRD pattern of PPy and **c** IR spectrum of PPy

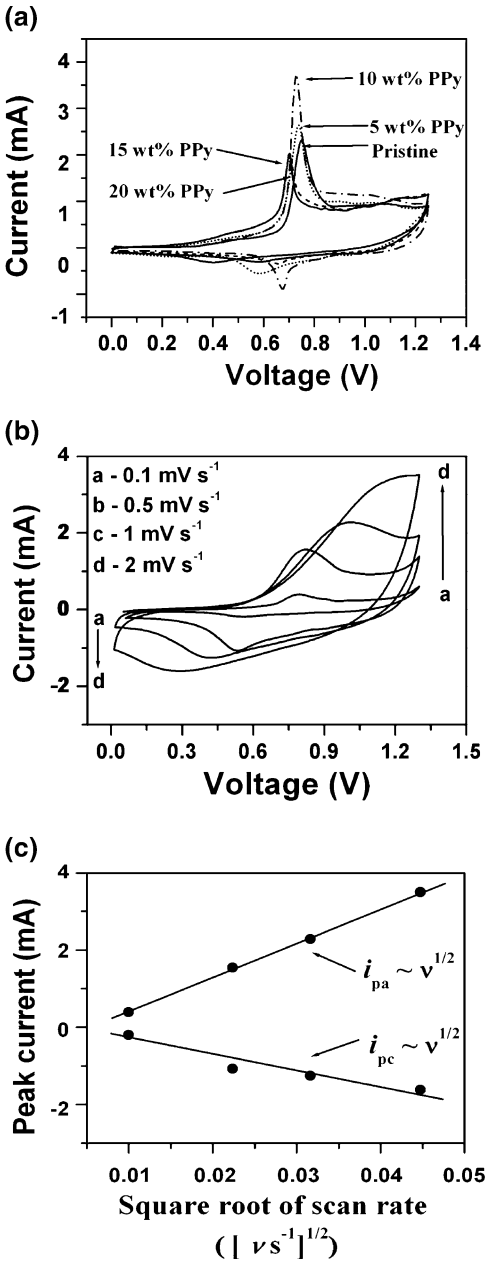

Fig. 3 **a** Cyclic voltammograms of pristine $LiNi_{1/3}Mn_{1/3}Co_{1/3}O_2$ and PPy-treated $LiNi_{1/3}Mn_{1/3}Co_{1/3}O_2$ composite electrodes in 5 M $LiNO_3$ electrolyte; scan rate 0.1 mV s^{-1}. **b** Cyclic voltammograms of 10 wt.% PPy–$LiNi_{1/3}Mn_{1/3}Co_{1/3}O_2$ composite electrode in 5 M $LiNO_3$ electrolyte at different scan rates. **c** Relationship between the peak currents and square root of scan rate calculated from Fig. 3b

Table 1 Peak potential differences at a scan rate of 0.1 mV s^{-1} calculated from Fig. 3a for pristine and PPy-treated electrodes

Sample	E_{pa}–E_{pc} (V)
Pristine $LiNi_{1/3}Mn_{1/3}Co_{1/3}O_2$	0.344
5 wt.% PPy–$LiNi_{1/3}Mn_{1/3}Co_{1/3}O_2$	0.156
10 wt.% PPy–$LiNi_{1/3}Mn_{1/3}Co_{1/3}O_2$	0.055
15 wt.% PPy–$LiNi_{1/3}Mn_{1/3}Co_{1/3}O_2$	0.028
20 wt.% PPy–$LiNi_{1/3}Mn_{1/3}Co_{1/3}O_2$	0.109

−0.50 V and de-intercalation peak at −0.24 V. The lithium intercalation and de-intercalation potentials in aqueous solution is almost the same as in organic electrolytes and the shape of the CV curve is same as reported in 1 M Li_2SO_4 [24]. Thus, it is possible to use LiV_3O_8 as an anode without evolution of hydrogen.

Figure 2a shows the cyclic voltammograms (CVs) recorded on Pt substrate during continuous cycling in a solution of 0.1 M pyrrole containing 0.1 mol dm^{-3} KCl. Figure 2b shows the XRD pattern of the synthesized PPy. The XRD pattern is in good agreement with the reported literature [25]. The lower angle maximum of 2θ at 24.5° means scattering from side-by-side pyrrole rings. Figure 2c shows the FT–IR spectrum of PPy. The characteristic bands of PPy can be observed at 1,550–1,650 cm^{-1} (C=C stretching vibration of doped PPy ring), 1,400 cm^{-1} (C–N stretching mode of doped PPy), 1,336 cm^{-1} (C–H or C–N in-plane deformation modes), 2,365 cm^{-1} (overtones and combinations of CH_2 and NH_2 stretching and wagging vibrations), and around 3,431 cm^{-1} (N–H and C–H stretching vibrations). Admixing of PPy with $LiNi_{1/3}Mn_{1/3}Co_{1/3}O_2$ cathode would reduce the particle-to-particle separation and also resistance which significantly enhances the electrical conductivity of the composites [26].

Electrochemical properties of PPy–$LiNi_{1/3}$ $Mn_{1/3}Co_{1/3}O_2$ composite electrode in 5 M $LiNO_3$ electrolyte

Cyclic voltammetry measurements were performed to examine the electrochemical properties of pristine $LiNi_{1/3}Mn_{1/3}Co_{1/3}O_2$ and PPy–$LiNi_{1/3}Mn_{1/3}Co_{1/3}O_2$ electrodes. The CV profiles obtained at room temperature in the first cycle are as shown in Fig. 3a. They all exhibited a pair of redox peaks. The CV profile of 10 wt.% PPy–$LiNi_{1/3}Mn_{1/3}Co_{1/3}O_2$ is found to exhibit more reversibility. As for cyclic voltammogram curves are considered, the potential interval between anodic peak and cathodic peak is an important parameter to evaluate the electrochemical reversibility [27]. As shown in Fig. 3a, 10 wt.% PPy–$LiNi_{1/3}Mn_{1/3}Co_{1/3}O_2$ composite electrode exhibited an anodic response at 0.73 V with 3.68 mA current and the corresponding cathodic response was at 0.675 V with −0.864 mA. The potential and current intervals were 0.055 V and 4.54 mA where as those for pristine electrode were 0.344 V and 2.6 mA, respectively. These results indicated that the overpotential for the de-intercalation and intercalation process was reduced after admixing polypyrrole with $LiNi_{1/3}Mn_{1/3}Co_{1/3}O_2$. The well-defined peaks and smaller values of potential intervals further showed the enhancement of electrode reaction reversibility by the addition of polypyrrole. The peak potential differences (E_{pa}–E_{pc}) of pristine, 5, 10, 15, and 20 wt.% PPy–$LiNi_{1/3}Mn_{1/3}Co_{1/3}O_2$ electrodes at 0.1 mV s^{-1} scan rates are listed in Table 1. It is clear from Table 1 that the potential intervals between anodic and cathodic peaks decrease with increase in PPy percentage up to 15 wt.% PPy. Figure 3b shows the cyclic voltammogrammes of 10 wt.% PPy–$LiNi_{1/3}Mn_{1/3}Co_{1/3}O_2$ composite obtained at different scan rates. The relationship between the peak currents (i_{pa}

Table 2 Peak potential differences at various scan rates calculated from Fig. 3b for 10 wt.% PPy–$LiNi_{1/3}$ $Mn_{1/3}Co_{1/3}O_2$

Scan rates	E_{pa}–E_{pc} (V)
0.1 mV s^{-1}	0.225
0.5 mV s^{-1}	0.283
1.0 mV s^{-1}	0.585
2.0 mV s^{-1}	0.967

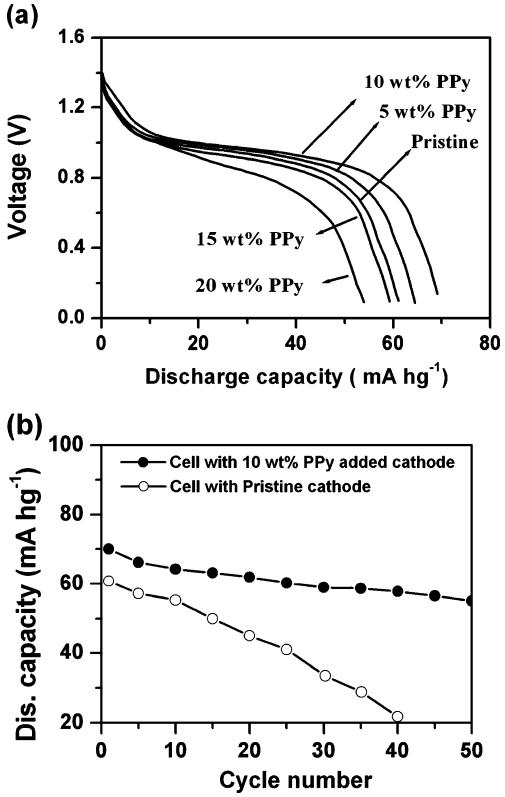

Fig. 4 **a** Initial discharge curves of pristine $LiNi_{1/3}Mn_{1/3}Co_{1/3}O_2$ and PPy–$LiNi_{1/3}Mn_{1/3}Co_{1/3}O_2$ composite electrodes. **b** Cycling performance of cells with pristine and 10 wt.% PPy–$LiNi_{1/3}Mn_{1/3}Co_{1/3}O_2$ electrodes

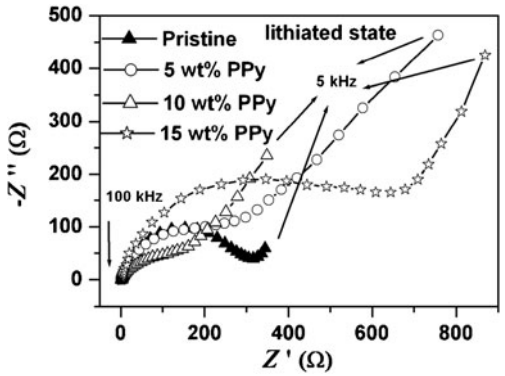

Fig. 5 AC impedance spectra of pristine and PPy-treated electrode in the fully lithiated state

and i_{pc}) and square root of scan rate ($\nu^{1/2}$) for anodic and cathodic peaks calculated from Fig. 3b is as shown in Fig. 3c. The peak currents are proportional to $\nu^{1/2}$ at different scan rates. This shows that the Li^+ de-intercalation/intercalation process taking place at the electrode is diffusion controlled process. At lower scan rates, the system yielded reversible waves while at higher scan rates (beyond 1 mV s^{-1}) irreversible behavior was observed. Table 2 shows the peak potential difference (ΔE_p) values at different scan rates for 10 wt.% PPy–$LiNi_{1/3}Mn_{1/3}Co_{1/3}O_2$ electrode.

According to the CV results, charge and discharge voltage of the LiV_3O_8/$LiNi_{1/3}Mn_{1/3}Co_{1/3}O_2$ cell were fixed between 0 and 1.4 V. The constant current applied was 0.2 mA cm^{-2}. Figure 4a shows the initial discharge curves of the cells LiV_3O_8/pristine $LiNi_{1/3}Mn_{1/3}Co_{1/3}O_2$ and LiV_3O_8/PPy–$LiNi_{1/3}Mn_{1/3}Co_{1/3}O_2$. The discharge capacity was calculated based on the total weight of the electro active materials $LiNi_{1/3}Mn_{1/3}Co_{1/3}O_2$ or (PPy+$LiNi_{1/3}Mn_{1/3}Co_{1/3}O_2$). The pristine $LiNi_{1/3}Mn_{1/3}Co_{1/3}O_2$ delivered an initial capacity of 60 mAh g^{-1}. The reasons for the low capacity achieved could be due to the cell voltage is close to the electrolysis voltage of water, a significant voltage drop during the initial stages of charge–discharge cycling and sharp inclining/declining charge/discharge curves which cause a rapid reach of voltage to the limiting values [28]. Polypyrrole addition improves the electrical conductivity of the composite electrodes and increases the utilization of $LiNi_{1/3}Mn_{1/3}Co_{1/3}O_2$ by inducing an enhanced specific capacity. The 10 wt.% PPy–$LiNi_{1/3}Mn_{1/3}Co_{1/3}O_2$ composite electrode exhibits better rate capability and high performance. The discharge capacity is found to be around 70 mAh g^{-1}, which is better than that at the pristine $LiNi_{1/3}Mn_{1/3}Co_{1/3}O_2$. Such an enhancement in the capacity (about 10 mAh g^{-1}) is reported in literature upon coating polypyrrole [20] and polyaniline [21] for $Li_xV_2O_5$ anode material; 15 and 20 wt.% PPy added composite electrodes delivered an initial capacity of 59 and 54 mAh g^{-1}, respectively, which are less than that of pristine $LiNi_{1/3}Mn_{1/3}Co_{1/3}O_2$. The decrease in the capacity of 15 and 20 wt.% PPy added composite electrodes can be explained as follows. With an increase in the amount of polypyrrole in the composite, more amount of PPy is present between $LiNi_{1/3}Mn_{1/3}Co_{1/3}O_2$ particles resulting in increased polymer material thickness between particles. Hence, the utilization of PPy will decrease with an increase in PPy in the composite. Its specific capacity decreases due to less utilization of PPy as polymer content increases. Based on the specific capacity, and utilization of PPy in the composites, it can be concluded that 10 wt.% represents an optimal amount of PPy in the composite [29] or the extra addition (15 and 20 wt.%) of PPy may just add to the dead mass of

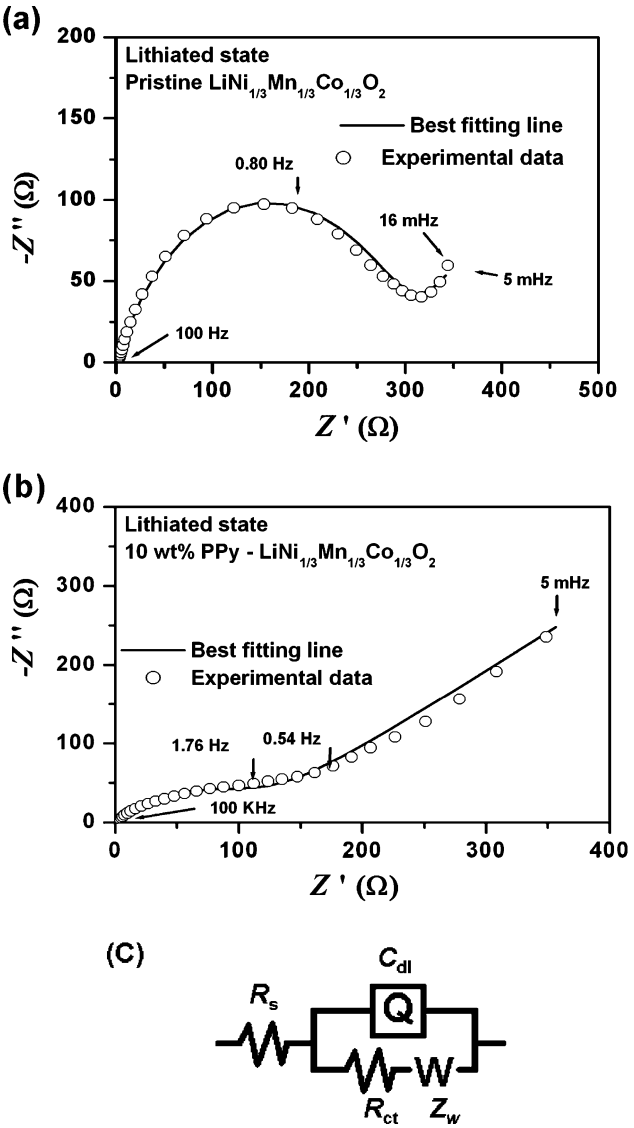

Fig. 6 **a** Experimental Nyquist plots of pristine $LiNi_{1/3}Mn_{1/3}Co_{1/3}O_2$. **b** 10 wt.% PPy–$LiNi_{1/3}Mn_{1/3}Co_{1/3}O_2$ and simulated results obtained in the fully lithiated state during discharge. **c** The equivalent circuit used to simulated the experimental impedance spectral data

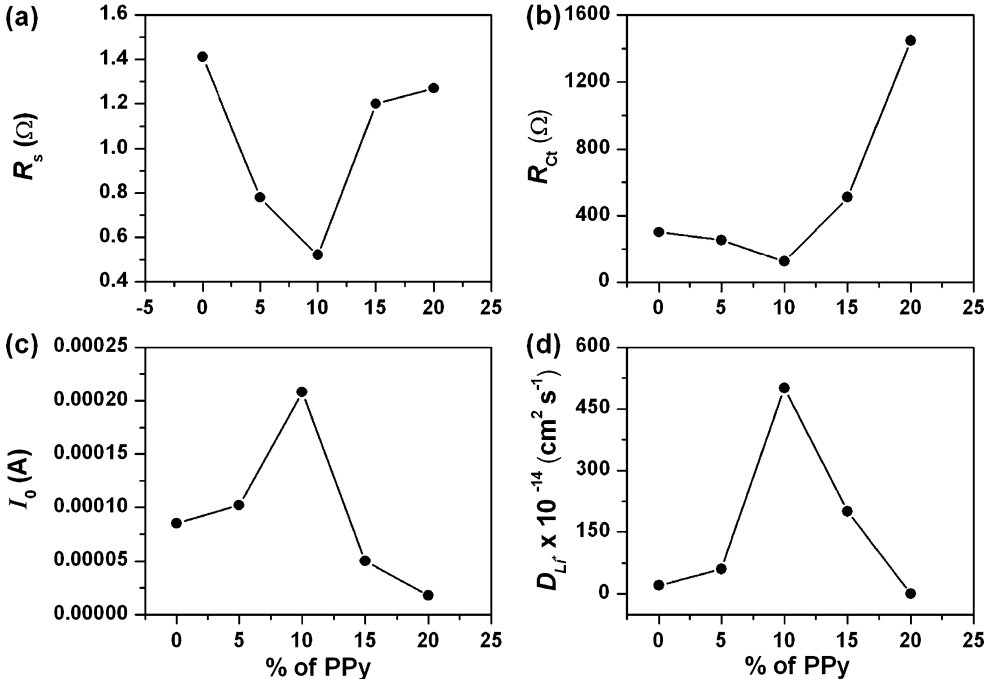

Fig. 7 Variation of R_s (**a**), R_{ct} (**b**), I_o (**c**), and D_{Li+} (**d**) in lithiated state with percentage of PPy vs SCE

the electrode which results in decrease of the capacity of the cell [30].

Figure 4b shows the cell performance of LiV_3O_8/pristine $LiNi_{1/3}Mn_{1/3}Co_{1/3}O_2$ and LiV_3O_8/10 wt.% PPy–$LiNi_{1/3}Mn_{1/3}Co_{1/3}O_2$ cells. The cell LiV_3O_8/pristine $LiNi_{1/3}Mn_{1/3}Co_{1/3}O_2$ exhibits 15 cycles with less than 16% capacity loss. After 15th cycle capacity faded. However, LiV_3O_8/10 wt.% PPy–$LiNi_{1/3}Mn_{1/3}Co_{1/3}O_2$ cell exhibited 15 cycles with a capacity loss of less than 7% and a capacity loss of about 17% at 30th cycle. It retained about 70% of the initial capacity after 50th cycle.

Electrochemical impedance spectroscopy (EIS) is an important technique to evaluate the kinetic parameters particularly the chemical diffusion coefficient of lithium ion. EIS was used to investigate the effect of PPy content on the lithium ion transfer reaction kinetics in PPy–$LiNi_{1/3}Mn_{1/3}Co_{1/3}O_2$ composite electrodes. Before taking the impedance spectra, the electrodes were cycled galvanostatically for 5 cycles to make sure if any formation of the stable of SEI layer on the surface of the electrode. The impedance spectra were recorded at two different states. Fully dis-

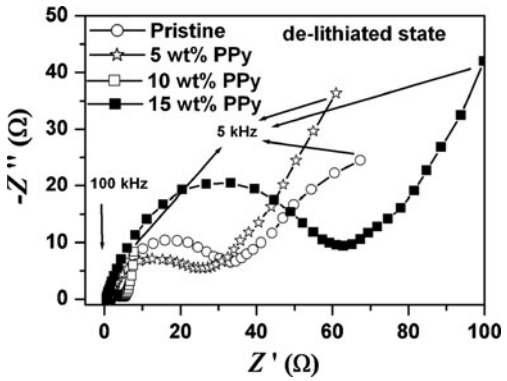

Fig. 8 AC impedance spectra of pristine and PPy-treated electrode in the fully de-lithiated state

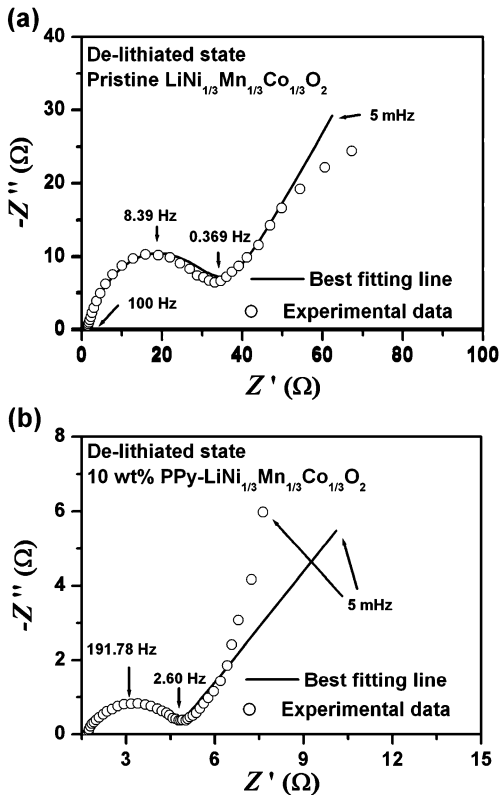

Fig. 9 **a** Experimental Nyquist plots of pristine $LiNi_{1/3}Mn_{1/3}Co_{1/3}O_2$. **b** 10 wt.% PPy–$LiNi_{1/3}Mn_{1/3}Co_{1/3}O_2$ and simulated results obtained in the fully de-lithiated state during charge

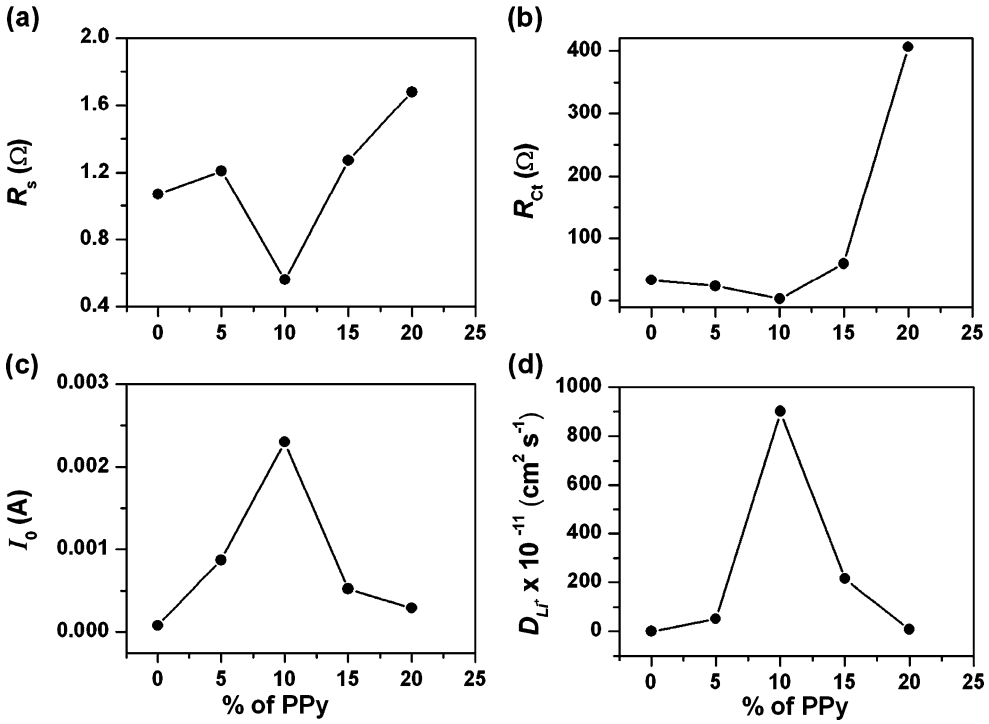

Fig. 10 Variation of R_s (**a**), R_{ct} (**b**), I_o(**c**), and D_{Li+} (**d**) in de-lithiated state with percentage of PPy vs SCE

charged (lithiated) state and in fully charged (de-lithiated) state according to the following reaction scheme in $LiNi_{1/3}Mn_{1/3}Co_{1/3}O_2$ electrode.

$$\text{Charge}: LiNi_{1/3}Mn_{1/3}Co_{1/3}O_2 \rightarrow Li_{(1-x)}Ni_{1/3}Mn_{1/3}Co_{1/3}O_2 + Li^+ + xe^{-1}(x<1) \quad (1)$$

$$\text{Discharge}: Li_{(1-x)}Ni_{1/3}Mn_{1/3}Co_{1/3}O_2 + Li^+ + xe^{-1} \rightarrow LiNi_{1/3}Mn_{1/3}Co_{1/3}O_2(x<1) \quad (2)$$

PPy is used as cathode which undergoes lithium insertion and de-insertion reactions in organic electrolytes through *n*-type doping mechanism [30]. However, it has been reported that in aqueous electrolytes, only *p*-type doping of PPy is possible. It is also proved that the redox peaks appeared for PPy in sat. Li_2SO_4 were not due to the intercalation/de-intercalation of Li^+ ions, but it was due to the doping and de-doping of SO_4^{2-} ion [31]. Therefore, polypyrrole may not undergo lithium insertion/de-insertion in aqueous electrolytes and it acts as a conductive additive and as binder upon addition to $LiNi_{1/3}Mn_{1/3}Co_{1/3}O_2$ cathode material. Figure 5 shows Nyquist plots of untreated and PPy–$LiNi_{1/3}Mn_{1/3}Co_{1/3}O_2$ composites in the lithiated state. The spectra show an intercept at high frequency region, a depressed semicircle in the high to middle frequency range, a Warburg type element (straight line with 45° angle to Z' axis) in the low frequency range and a capacitive line. The intercept impedance on the Z' axis represents the ohmic resistance of the electrolyte and electrode. The high frequency semicircle is related to the charge-transfer through the electrode–electrolyte interface, the Warburg region is assigned to solid state diffusion of lithium ions through the solid matrix of the cathode material. The semicircle becomes much more suppressed and the inclined line in the low frequency range almost disappears in 10 wt.% PPy modified electrode. Decreased diameter of the semicircle and the minimum of the semicircles when all the values of $-Z''$ are related indicates the improved charge transfer process at 10 wt.% PPy electrode. Ohmic resistances of PPy-treated electrodes were smaller than that of the untreated $LiNi_{1/3}Mn_{1/3}Co_{1/3}O_2$ suggesting a reduced resistance between electrolyte and electrode due to the addition of PPy to $LiNi_{1/3}Mn_{1/3}Co_{1/3}O_2$.

Figure 6a and b shows the best fitting between experimental and simulated data using the equivalent circuit shown in Fig. 6c for pristine and PPy-treated composite electrodes respectively. In the equivalent circuit, R_s represents ohmic resistance of the solution, R_{ct} is the charge transfer resistance, Q the double layer capacitance, and Z_w the Warburg impedance. To get better fitting results, the pure capacitor in the Randle's equivalent circuit is replaced by constant phase elements (CPE, Q). A CPE is used when the impedance spectra exhibit low frequency dispersion. It is suggested that such dispersion could be caused by the film—substrate interface, roughness, porosity, or homogeneity [32–34]. Figure 7 shows the variation of kinetic

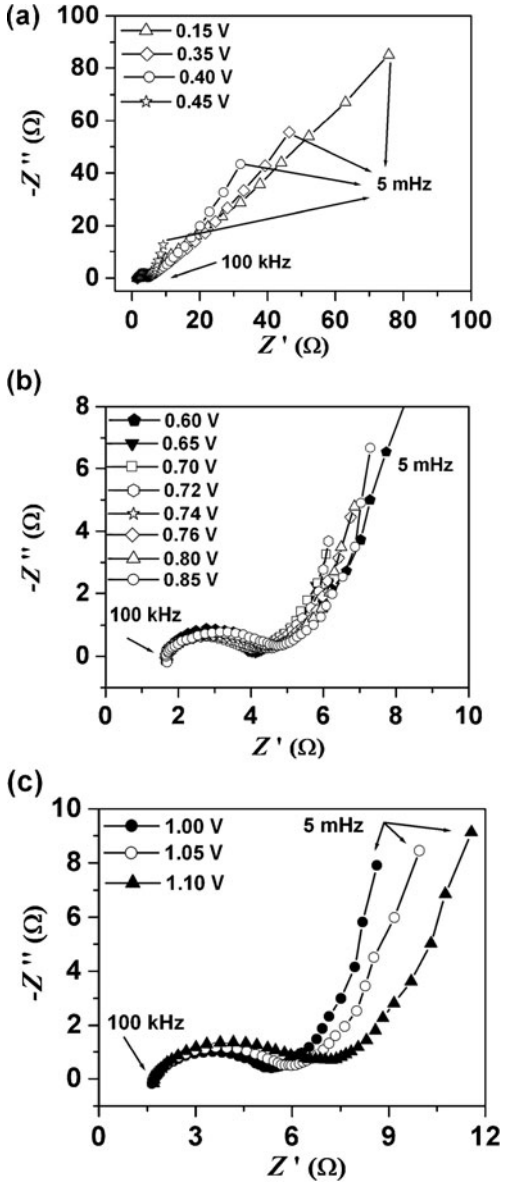

Fig. 11 Nyquist plots of 10 wt.% PPy–$LiNi_{1/3}Mn_{1/3}Co_{1/3}O_2$ composite electrode in different potential domains during charge. **a** Before lithium de-insertion, **b** the middle of lithium de-insertion and **c** towards the end of lithium de-insertion

parameters in the lithiated state for pristine and PPy treated $LiNi_{1/3}Mn_{1/3}Co_{1/3}O_2$ electrodes. The Butler–Volmer equation can be liberalized when the amplitude of the potential perturbation signal is less than 10 mV, and the exchange current I_0 is calculated according to the following equation.

$$I_0 = RT/\mathrm{n}FR_{\mathrm{ct}} \tag{3}$$

The diffusion coefficient of Li ion, $D_{\mathrm{Li+}}$, can be calculated from the plots in the low frequency region according to the following equation:

$$D_{\mathrm{Li+}} = 0.5[V_{\mathrm{m}}(\mathrm{d}E/\mathrm{d}x)/nFAZ_{\mathrm{w}}]^2 \tag{4}$$

where V_{m} is molar volume of $LiNi_{1/3}Mn_{1/3}Co_{1/3}O_2$ composite which is 42.3 cm^3/mol. n is number of electrons per molecule, A is electrode surface area, F Faraday constant, and Z_{w} Warburg factor. $\mathrm{d}E/\mathrm{d}x$ values were calculated from the charge–discharge curves. The chemical diffusion coefficient of lithium ions shows an increased value for 10 wt.% PPy–$LiNi_{1/3}Mn_{1/3}Co_{1/3}O_2$. R_{s} values of PPy-modified electrodes are found to be lower than that of pristine electrode. R_{ct} that represents the diameter of the semicircle decreases with the percentage of PPy added and is lowest for 10 wt.% PPy-modified electrode. Corresponding I_0 increases with polypyrrole addition, and it reaches to a maximum value of 0.22 mA for 10 wt.% PPy and then decreases. The important kinetic parameter $D_{\mathrm{Li+}}$ exhibits a maximum at 10 wt.% PPy addition indicating an increase in the diffusion coefficient of lithium ions. The increase in the resistance (R_{ct}) at higher percentages of PPy (15 and 20 wt. %) may be due to the increased thickness of the polymer between the particles of electrode material. Decreased ionic conductance or slow diffusion of dopants in thick polypyrrole films have been reported [35]. Also, Li et.al [36] have shown that the increase of polyaniline conducting polymer film thickness blocks electron transfer between the solution and electrode. Therefore, as the percentage of PPy increases above 10 wt.%, it may offer resistance for the diffusion of lithium ions. In addition to this, since the percentage of PPy is more, the PPy polymer present at the surface of the electrode may form a blocking layer at the interface between the electrode and the solution and offer some resistance for the electron-charge-transfer process.

Figure 8 shows the Nyquist plots of untreated and PPy-treated $LiNi_{1/3}Mn_{1/3}Co_{1/3}O_2$ composites in the delithiated state. The diameter of the semicircle and also the impedance when all the $-Z''$ values are compared is found to be low for 10 wt.% PPy–$LiNi_{1/3}Mn_{1/3}Co_{1/3}O_2$ electrode. Figure 9a and b shows the best fitting of experimental and simulated data using the equivalent circuit shown in Fig. 6c for pristine and PPy-treated composite electrodes, respectively, in the delithiated state. The diameter of the semicircle is about ten times lower for 10 wt.% PPy-added electrode compared to that for the pristine electrode which indicates the decreased charge transfer resistance due to the addition of polypyrrole. The variation of kinetic parameters with percentage of polypyrrole in the de-lithiated state show the same trend as it is observed for the lithiated state, and it is as shown in Fig. 10.

Electrochemical de-intercalation/intercalation of lithium ions in PPy–$LiNi_{1/3}Mn_{1/3}Co_{1/3}O_2$ composite electrode

Figure 11a and b demonstrates the typical Nyquist plots of the AC impedance spectra obtained for 10 wt.% PPy–$LiNi_{1/3}$

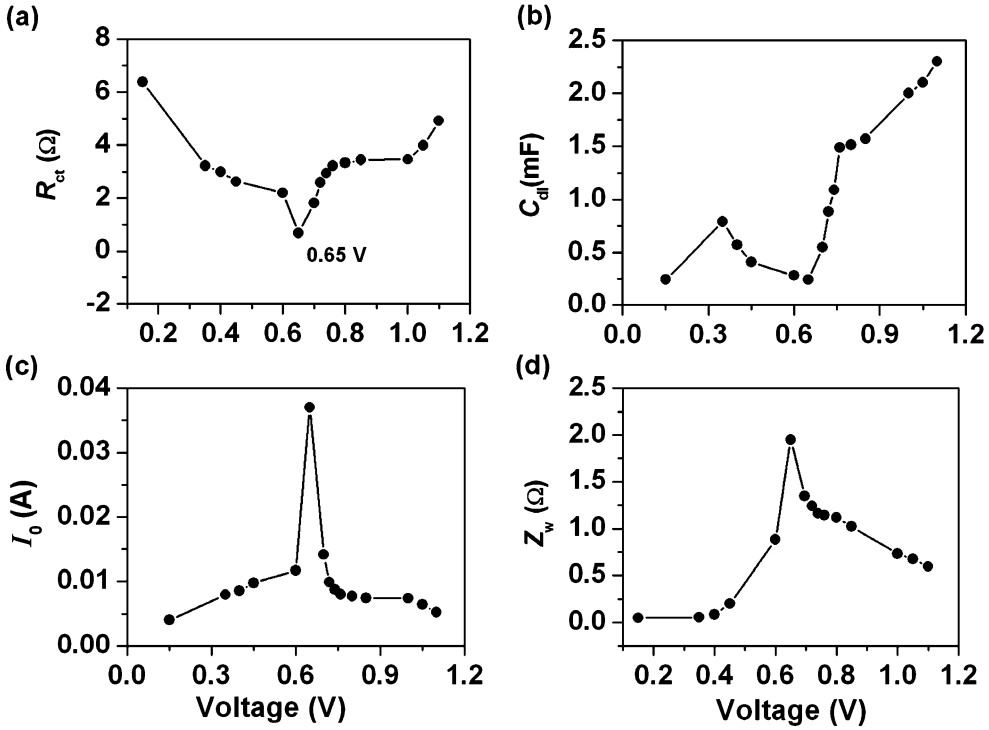

Fig. 12 Variation of kinetic parameters 10 wt.% PPy–$LiNi_{1/3}Mn_{1/3}Co_{1/3}O_2$ with the charge voltages

$Mn_{1/3}Co_{1/3}O_2$ composite electrode at different potential domains viz before lithium de-intercalation, middle of lithium intercalation, and after lithium intercalation, respectively. The AC impedance spectroscopy was performed at each of the applied potentials during charge. All the spectra are characterized by a semicircle in the high to medium frequency region corresponding to the charge transfer process, a Warburg type element which represents the solid-state diffusion of lithium ions and capacitive behavior at the lower frequency region which may be due to the roughness and porosity of the surface of the composite electrode. The kinetic parameters of the lithium de-intercalation process from 10 wt.% PPy–$LiNi_{1/3}Mn_{1/3}Co_{1/3}O_2$ were evaluated by simulating the experimental impedance plots with the equivalent circuit shown in Fig. 6c. The interpretation of the circuit has already discussed in the previous section. Figure 12 shows the variation of kinetic parameters during charge with the applied potential. One of the important kinetic parameters of these insertion materials is R_{ct}. As seen from the figure, charge-transfer resistance decreases with increase in potential, and it reaches to a minimum at 0.65 V vs SCE which is near the peak potential (0.73 V) observed in the CV profile of 10 wt.% PPy–$LiNi_{1/3}Mn_{1/3}Co_{1/3}O_2$ implying favorable kinetic conditions for de-intercalation. Correspondingly, the exchange current, I_0, increases with charge voltage and reaches a maximum at 0.65 V when charge-transfer resistance is lowest. R_s stays constant at 1.60 Ω as expected because the solution composition and conductance do not change. C_{dl} decreases at the beginning of lithium de-insertion perhaps due to the absence of passivity film on the surface of 10 wt.% PPy–$LiNi_{1/3}Mn_{1/3}Co_{1/3}O_2$ electrode and then increases. Figure 13 shows the Nyquist plots of ac impedance spectra obtained for 10 wt.% PPy–$LiNi_{1/3}Mn_{1/3}Co_{1/3}O_2$ composite electrode during lithium ion insertion (discharge). As seen in figure, there is a continuous change in the diameter of the high to medium frequency semicircle during lithium intercalation. Figure 14 shows the variation of kinetic parameters with the applied potential during discharge. We have recently reported [37] a similar trend in the variation of kinetic parameters with applied potential for lithium intercalation into $LiMn_2PO_4$ spinel from aqueous 2 M Li_2SO_4 electrolyte. The low values of charge-transfer resistances obtained during lithium intercalation and de-intercalation processes for 10 wt.% PPy–$LiNi_{1/3}Mn_{1/3}Co_{1/3}O_2$ com-

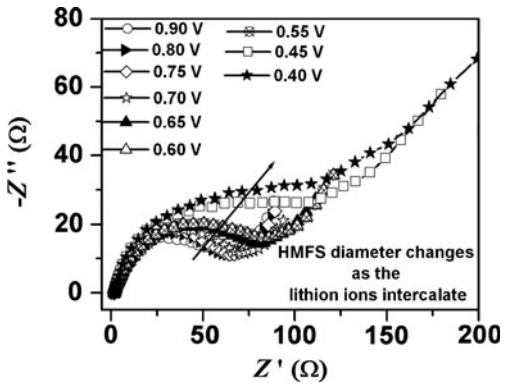

Fig. 13 Nyquist plots of 10 wt.% PPy–$LiNi_{1/3}Mn_{1/3}Co_{1/3}O_2$ composite electrode at different potentials during discharge

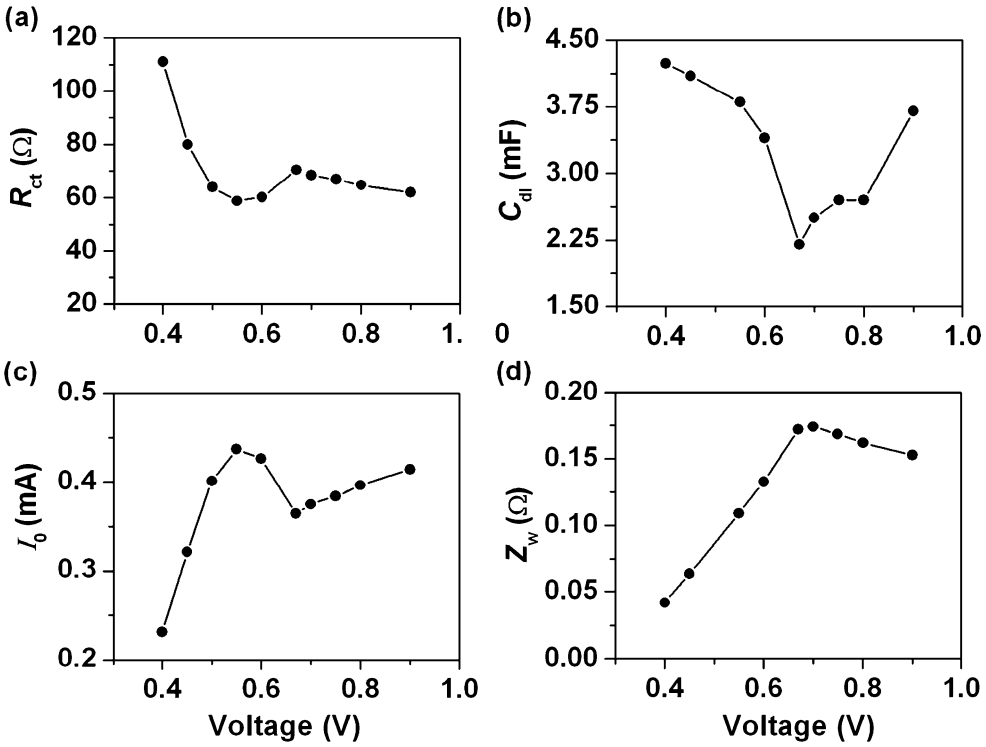

Fig. 14 Variation of kinetic parameters 10 wt.% PPy–$LiNi_{1/3}Mn_{1/3}Co_{1/3}O_2$ with the discharge voltages

pared to that for pristine $LiNi_{1/3}Mn_{1/3}Co_{1/3}O_2$ (see Figs. 7 and 10) indicates that the enhanced charge transfer kinetics results from the conductive PPy addition to $LiNi_{1/3}Mn_{1/3}Co_{1/3}O_2$ cathode material.

Conclusions

$LiNi_{1/3}Mn_{1/3}Co_{1/3}O_2$ cathode material was successfully prepared by RAPET method. Addition of polypyrrole is an effective way to improve the electrochemical properties of $LiNi_{1/3}Mn_{1/3}Co_{1/3}O_2$ cathode material. Polypyrrole could enhance the ionic conductivity of $LiNi_{1/3}Mn_{1/3}Co_{1/3}O_2$ material and produce good electrical contact between the particles. Cyclic voltammetry, electrochemical impedance studies provide strong evidence for improved reaction reversibility of $LiNi_{1/3}Mn_{1/3}Co_{1/3}O_2$ cathode with polypyrrole addition. 10 wt.% PPy has better electrochemical performance than pristine, 5, 15, and 20 wt.% PPy-modified $LiNi_{1/3}Mn_{1/3}Co_{1/3}O_2$ composite electrodes. The cell with 10 wt.% PPy-added cathode shows significant improvement in the electrochemical performance compared with that having pristine cathode. The capacity remains about 70% of original value after 50 cycles while for cell with pristine cathode only about 28% of original capacity remains after 40 cycles. The drastic decrease in the charge-transfer resistances obtained from EIS technique during lithium intercalation and de-intercalation processes for 10 wt.% PPy–$LiNi_{1/3}Mn_{1/3}Co_{1/3}O_2$ compared to that for pristine $LiNi_{1/3}Mn_{1/3}Co_{1/3}O_2$ proves that the enhanced charge transfer kinetics results from the conductive PPy addition to $LiNi_{1/3}Mn_{1/3}Co_{1/3}O_2$ cathode material.

Acknowledgements The authors gratefully acknowledge the financial support from the Department of Science and Technology, Government of India. Authors wish to thank Sri. A. V. S. Murthy, honorary secretary, Rashtreeya Sikshana Samiti Trust, Bangalore, and Dr. P. Yashoda, Principal, S.S.M.R.V. Degree College, for their support and encouragement. We also thank the Department of Chemistry, St. Joseph's College, Bangalore for XRD data. R.B. Shivashankaraiah thank the management of Dayananda Sagar Institution, Bangalore for giving permission to carryout research work.

References

1. Li W, Dahn JR, Wainwright DS (1994) Science 264:1115–1118
2. Manjunatha H, Suresh GS, Venkatesha TV (2011) J Solid State Electrochem 15(3):431–445
3. Wang P, Yang H, Yang HQ (1996) J Power Sources 63:275–278
4. Yang HQ, Li DP, Han S (1996) J Power Sources 58:221–224
5. Wang GX, Zhong S, Bradhurst DH (1998) J Power Sources 74:198–201
6. Eftikhari A (2001) Electrochim Acta 47:495–499
7. Lu Z, Macneil DD, Dahn JR (2001) Electrochem Solid State Lett 4:A200–A203
8. Cho TH, Shiosaki Y, Noguchi H (2006) J Power Sources 159:1322–1327
9. Ozhuku T, Makimura Y (2001) Chem Lett 30:642–643
10. Li DC, Muta T, Zhang LQ, Yoshio M, Noguchi H (2004) J Power Sources 132:150–155
11. Yabuuchi N, Ozhuku T (2003) J Power Sources 171:119–121
12. Shaju KM, Subba Rao GV, Choudari BVR (2002) Electrochim Acta 48:145–151

13. Belharouak I, Sun YK, Li J, Amine K (2003) J Power Sources 123:247–252
14. Choi JJ, Manthiram AA (2005) J Electrochem Soc 152:A1714–A1718
15. Luo XF, Luo XY, Wang XY, Liao LL, Gamboa S, Sebastian PJ (2006) J Power Sources 158:654–658
16. Fuji Y, Miura H, Suzuki N, Shoji T, Nakayama N (2007) J Power Sources 171:894–903
17. Zhang WW, Liu HX, Hu CC, Zhu XJ, Li YX (2008) Rare Metals 27:158–164
18. Koyama Y, Tanaka I, Adachi H, Makimura Y, Ozhuka T (2003) J Power Sources 119–121:644–648
19. Chung, Lu H, Lin YK (2009) J Power Sources 189:40–44
20. Wang H, Zeng Y, Huang K, Liu S, Chen L (2007) Electrochim Acta 52:5102
21. Wang H, Huang K, Zeng Y, Zhao F, Chen L (2007) Electrochem Solid-State Lett 10(9):A199
22. Levin EM, McMurdie HF (1975) Phase diagrams for Ceramics, Vol III. American Chemical Society, Washington, DC, p 49
23. Wadslay AD (1957) Acta Cryst 10:261–271
24. Kohler J, Makihara H, Uegaito H, Inoue H, Toki M (2000) Electrochim Acta 46:59–65
25. Liu Y-C, Chuang TC (2003) J Phys Chem B 107:12383–12386
26. Wang GJ, Yang LC, Qu QT, Wang B, Wu YP, Holze R (2010) J Solid State Electrochem 14:865–869
27. Ni JF, Zhon HH, Chen JJ, Zhang XX (2005) Mater Lett 59:2361–2365
28. Sinha NN, Raghupathy P, Vasan HN (2008) Munichandraiah N 3:691–710
29. Ramaraja PR, Basker V, Bala H, Popov BN (2003) J Power Sources 124:197–203
30. Wang GX, Yang L, Wang JZ, Bewlay S, Liu HK (2005) Electrochim Acta 50:4649–4654
31. Wang GJ, Yang LC, Qu QT, Wang B (2010) J Solid State Electrochem. doi:10.1007/s10008-009-0869-3
32. Ho C, Raistrick ID, Huggins RA (2000) J Electrochem Soc 147:2044–2049
33. Pajkossy T (1994) J Electroanal Chem 364:111–125
34. Pajkossy T, Wandlowski T, Neves RS (1996) J Electroanal Chem 414:209–210
35. Osaka T, Naoi K, Ogano S (1987) J Electrochem Soc 134:2096–2102
36. Li M, Jing L (2007) Electrochim acta 52:3250–3257
37. Manjunatha H, Mahesh KC, Suresh GS, Venkatesha TV (2011) Electrochim Acta 56:1439–1446